Quasi-two-dimensional massless Dirac fermions in $CaMnSb_2$

J. B. He,[1,2] Y. Fu,[2] L. X. Zhao,[1] H. Liang,[1] D. Chen,[1] Y. M. Leng,[2] X. M. Wang,[1] J. Li,[1] S. Zhang,[1] M. Q. Xue,[1] C. H. Li,[1] P. Zhang,[2] Z. A. Ren,[1,4] and G. F. Chen[1,3,4,*]

[1]*Institute of Physics and Beijing National Laboratory for Condensed Matter Physics, Chinese Academy of Sciences, Beijing 100190, China*

[2]*College of Physics and Electronic Engineering, Nanyang Normal University, Nanyang 473061, China*

[3]*School of Physical Sciences, University of Chinese Academy of Sciences, Beijing 100190, China*

[4]*Collaborative Innovation Center of Quantum Matter, Beijing 100190, China*

(Received 26 September 2016; revised manuscript received 6 December 2016; published 17 January 2017)

We report a study of the magnetic and magnetotransport properties of layered transition-metal pnictide $CaMnSb_2$. $CaMnSb_2$ is a quasi-two-dimensional system with an orthorhombic crystal structure, containing two distinct layers of a distorted Sb square sheet and an edge-sharing $MnSb_4$ tetrahedron. It was found that $CaMnSb_2$ orders antiferromagnetically below $T_N = 302$ K and exhibits the expected highly anisotropic magnetic and electrical transport properties. At low temperatures and high fields, we observed quantum oscillations in both magnetization and resistivity, which reveal the multiband Fermi surfaces with very small cross-sectional areas. Nonzero Berry phase, very small cyclotron mass, and high carrier mobility indicate the existence of nearly massless Dirac fermions in $CaMnSb_2$.

DOI: 10.1103/PhysRevB.95.045128

Topological materials, especially Dirac and Weyl semimetals, have received increasing attention in recent years because of their special physical properties and potential applications [1–12]. In such systems, the electron transport is essentially governed by relativistic Dirac or Weyl equations, which leads to large linear magnetoresistance (MR), nontrivial Berry phase, quantum Hall effect, and/or negative magnetoresistance [1–7,11,12].

Recently, both theoretical and experimental investigations indicated that Dirac or Weyl fermions host in the compounds with a two-dimensional Bi/Sb layer such as $AMnBi_2$ and $AMnSb_2$ (A = Ca, Sr, Ba, Eu, and Yb) [13–35]. $AMnBi_2$ are layered compounds with tetragonal crystal structure, containing alternate layers of a Bi square sheet and an edge-sharing $MnBi_4$ tetrahedron, which are separated by A ions. The space group changes from *P4/nmm* for $(Ca/Yb)MnBi_2$ to *I4/mmm* for $(Sr/Ba/Eu)MnBi_2$ with the change of A ion radii, resulting in the arrangement of A ions (above and below the Bi square net) changing from staggered arrangement to a coincident one [13–21]. Both band-structure calculations and angle-resolved photoemission measurements indicated that the local arrangement of A ions and spin-orbit coupling play important roles for the Dirac cone formation [23,24].

$BaMnSb_2$ is isostructural with $BaMnBi_2$ and also hosts Dirac fermions [33,34]. However, $(Ca/Sr)MnSb_2$ crystalizes in an orthorhombic *Pnma* structure [Fig. 1(a)]. The Sb square net in $(Ca/Sr)MnSb_2$ is slightly distorted to give a zig-zag chainlike structure along the b axis [Fig. 1(b)], which is different from the arrangement of the Bi/Sb square net in $AMnBi_2$ and $BaMnSb_2$ [Fig. 1(c)] [35,36]. Surprisingly, $Sr_{1-y}Mn_{1-z}Sb_2$ exhibits ferromagnetism [35], in contrast with the observed antiferromagnetic ground states in $AMnBi_2$ [13–21]. For $CaMnSb_2$, the crystal structure has been characterized by Brechtel *et al.* three decades ago [36]; however, no investigation of physical properties has been performed. We report here various physical properties of $CaMnSb_2$ single crystals. Our results show that $CaMnSb_2$ is a quasi-two-dimensional system and hosts nearly massless Dirac fermions.

High-quality single crystals of $CaMnSb_2$ were grown by flux method. The starting materials, Ca, Mn, and Sb, were mixed in the ratio of Ca : Mn : Sb = 1 : 1 : 4, put into an alumina crucible, and sealed in a quartz tube. The quartz tube was heated slowly to 850°C, held for 20 h, and then cooled to 620°C at a rate of 1°C/h, where the flux was decanted using a centrifuge. Shiny platelike single crystals with a typical dimension of $5 \times 5 \times 1$ mm^3 were obtained. The crystal structure was characterized by x-ray diffraction (XRD) using a PANalytical diffractometer with Cu K_α radiation at room temperature. The elemental compositions were checked by Oxford X-Max energy dispersive x-ray (EDX) spectroscopy analysis in a Hitachi S-4800 scanning electron microscope. Magnetic and electrical transport measurements were performed on a Quantum Design MPMS-7 T SQUID VSM and PPMS-9 T system, respectively.

The powder XRD pattern of $CaMnSb_2$ (not shown here) can be well indexed to the orthorhombic *Pnma* structure with the lattice parameters $a = 22.09$ Å, $b = 4.32$ Å, and $c = 4.35$ Å, which are in agreement with the previously reported values [36]. Figure 1(d) shows the single-crystal XRD pattern with (h00) reflections, indicating that the crystal is cleaved along the bc plane. The atomic ratio determined from EDX is Ca : Mn : Sb = 0.98 : 0.95 : 2, which is very close to the stoichiometry of $CaMnSb_2$.

Figure 2 presents the temperature dependence of magnetic susceptibility $\chi(T)$ for different crystallographic directions. Above 302 K, the linear temperature dependence of $\chi(T)$ for both $B\|a$ and $B\|bc$ suggests that strong magnetic correlations exist in high temperature [13,15,20]. Just below 302 K, $\chi(T)$ shows a sharp decrease for $B\|a$ while almost keeping a constant for $B\|bc$, indicating that a long-range antiferromagnetic order develops and the magnetic easy axis is along the a axis. With further cooling down to 270 K, there is another rapid drop and a splitting between zero-field-cooled (ZFC) and field-cooled (FC) mode for $B\|a$, but no other anomaly occurs for $B\|bc$. This phenomenon is also observed in $(Ca/Sr)MnBi_2$

*gfchen@iphy.ac.cn

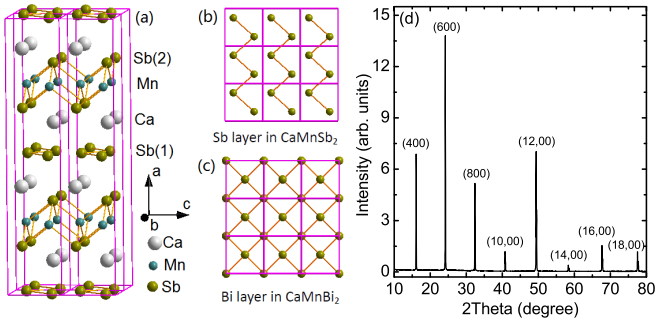

FIG. 1. (a) The crystal structure of $CaMnSb_2$ with a space group of *Pnma*. (b) Schematic of the distorted Sb square net layer in $CaMnSb_2$, where Sb atoms form zig-zag chains along the *b* axis. (c) Schematic of the Bi square net layer in $CaMnBi_2$. (d) Single-crystal XRD pattern of $CaMnSb_2$.

and the neutron-diffraction experiment indicates that the observed anomaly below the antiferromagnetic order may be due to domain formation or disorder [26,27]. Although ferromagnetism caused by deficiency has been observed in (Sr/Ba)$MnSb_2$ [34,35], no ferromagnetic response has been detected in any of our $CaMnSb_2$ single crystals. This implies that there is no obvious deficiency in $CaMnSb_2$ single crystals obtained in our experiment, which is consistent with the result of EDX. Magnetization isotherms at 2 K for two orientations are shown in the inset of Fig. 2. De Haas–van Alphen (dHvA) oscillations are clearly observed in fields as low as 1 T for $B\|a$, superimposed on a linear background. The linear dependence of the magnetization with field is in agreement with an antiferromagnetic ground state in $CaMnSb_2$.

Since the dHvA effect is one of the most powerful experimental probes to study the Fermi-surface (FS) properties, we measured a series of magnetization M for $B\|a$ at various temperatures for extracting the oscillations. Figure 3(a) shows the reciprocal of magnetic field ($1/B$) dependence of the oscillatory parts $\Delta M = M - \langle M \rangle$, where $\langle M \rangle$ is the smooth background. The fast Fourier transform (FFT) of

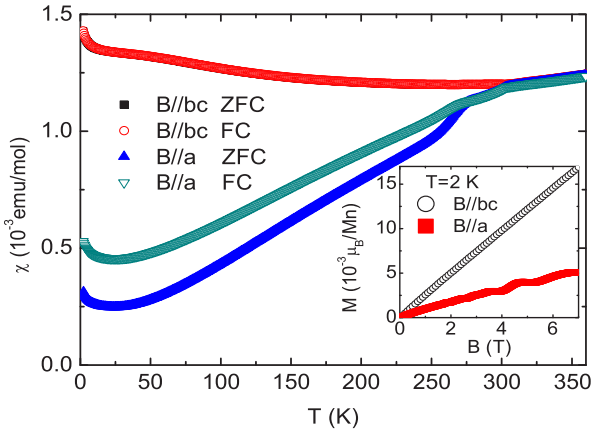

FIG. 2. Temperature dependence of magnetic susceptibility for the $CaMnSb_2$ single crystal with magnetic field $B = 1$ T for $B\|a$ and $B\|bc$ in both zero-field-cooled (ZFC) and field-cooled (FC) mode. The inset shows magnetization M vs magnetic field B for $B\|a$ and $B\|bc$ at 2 K.

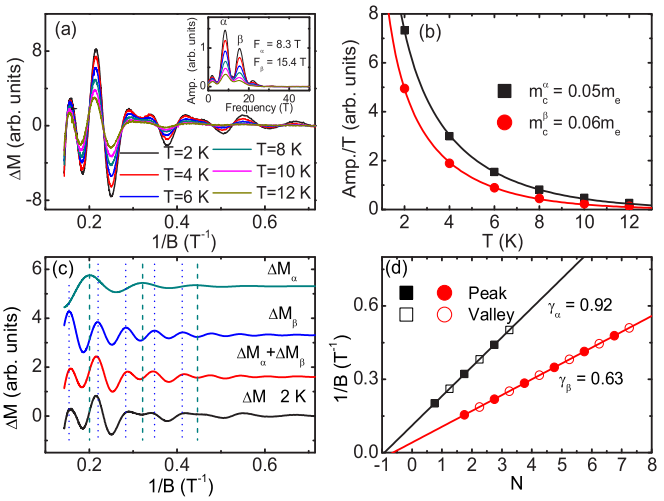

FIG. 3. (a) The reciprocal of magnetic field dependence of dHvA oscillations ΔM at various temperatures for $B\|a$. The inset shows FFT spectra of dHvA oscillations. (b) Temperature dependence of dHvA oscillation amplitude (Amp.) plotted as Amp./T vs T for two frequencies. The solid line is the fitting results giving cyclotron mass. The values of Amp. and B are determined from the FFT results in the fitting process. (c) The experimental data ΔM and the fitting results (i.e., $\Delta M_\alpha + \Delta M_\beta$, ΔM_α, and ΔM_β) by two oscillatory frequency components using the Lifshitz-Kosevich formula. The vertical dark cyan dash and blue dotted lines are the peak positions of ΔM_α and ΔM_β, respectively. (d) Landau-level index plots $1/B$ vs N for two frequencies.

the oscillatory data is shown in the inset of Fig. 3(a). Two fundamental frequencies, $F_\alpha = 8.3$ T and $F_\beta = 15.4$ T, are clearly detected. Using the Onsager relation $F = (\Phi_0/2\pi^2)A_F$ (where Φ_0 is the flux quantum and A_F is the cross-sectional area of the FS), it is calculated that the corresponding A_F are 0.08 and 0.15 nm^{-2}, respectively, which are very small and only about 0.04 and 0.07% of the first Brillouin zone. Figure 3(b) shows the temperature dependence of the oscillating amplitudes (Amp.). By fitting the thermal damping term $R_T = \frac{2\pi^2 k_B T m_c/\hbar eB}{sinh(2\pi^2 k_B T m_c/\hbar eB)} \propto$ Amp. (where m_c is the cyclotron effective mass, k_B is Boltzman's constant, $\hbar$ is Planck's constant divided by 2π, and e is the charge on the bare electron), the cyclotron effective masses are estimated to be $0.05m_e$ and $0.06m_e$ (m_e is the bare electronic mass), respectively. The values are comparable with that of $BaMnSb_2$ ($0.052 \sim 0.058m_e$) [34] but smaller than those of $SrMnSb_2$ ($0.14m_e$) [35] and $AMnBi_2$ ($0.1 \sim 0.4m_e$) [13–15,17,20].

The nontrivial Berry phase of π is an important characteristic of Dirac fermions which can also be revealed in the quantum oscillations measurements. In general, the dHvA oscillations can be expressed with the Lifshitz-Kosevich formula [37,38]:

$$\Delta M \propto -B^{1/2} R_T R_D \sin[2\pi(F/B - \gamma)], \quad (1)$$

where $R_D = \exp(-\frac{2\pi^2 k_B T_D m_c}{\hbar eB})$ is the Dingle damping term, T_D is Dingle temperature, and $\gamma = \frac{1}{2} - \frac{\phi_B}{2\pi}$ is a phase factor related to the Berry phase (ϕ_B). It is well known that γ is expected to be zero or one for nontrivial Berry phase but 1/2 for the trivial Berry phase, which can be extracted from the Landau-level fan diagram. Figure 3(c) shows the results fitted by two oscillatory

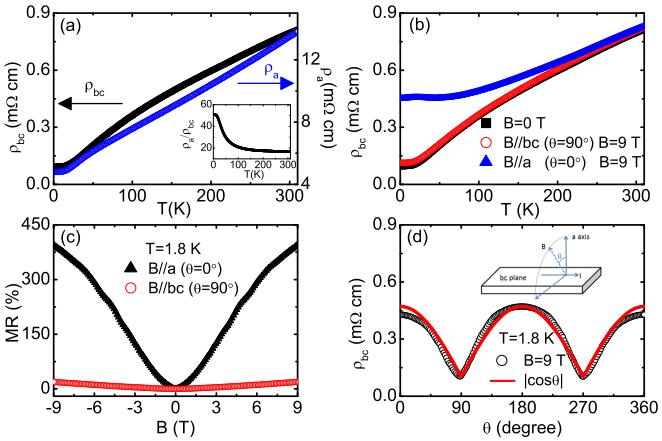

FIG. 4. (a) Temperature dependence of in-plane resistivity $\rho_{bc}(T)$ and out-of-plane resistivity $\rho_a(T)$. The inset shows temperature dependence of the $\rho_a(T)/\rho_{bc}(T)$ ratio. (b) Temperature dependence of in-plane resistivity $\rho_{bc}(T)$ in the field of 0 and 9 T for both $B\|a$ and $B\|bc$. (c) Magnetic field dependence of magnetoresistance (MR) at 1.8 K for both $B\|a$ and $B\|bc$. (d) The in-plane resistivity ρ_{bc} as a function of the tilt angle θ at 1.8 K in a magnetic field of 9 T. The red solid line is the fitting curve using $|\cos\theta|$. The inset shows the configuration of measurement.

frequency components (ΔM_α and ΔM_β). The valleys and peaks of oscillations can be designated with the Landau-level index of $N - 3/4$ and $N - 1/4$, respectively, which are plotted against the reciprocal of magnetic field $1/B$ in Fig. 3(d). The linear extrapolation of the plot yields the values of γ_α and γ_β to be 0.92 and 0.63, respectively. Considering the phase offset related to the systematic dimensions and the experimental errors, it is reasonable to assume that γ_α is closed to the expected value of the nontrivial Berry phase, whereas γ_β is closed to that of the trivial Berry phase. The observed nontrivial Berry phase seems to indicate the existence of Dirac fermions in $CaMnSb_2$.

Figure 4(a) shows the temperature dependence of in-plane resistivity $\rho_{bc}(T)$ and out-of-plane resistivity $\rho_a(T)$. Both $\rho_{bc}(T)$ and $\rho_a(T)$ decrease with decreasing temperature and exhibit metallic behavior down to 1.8 K. The anisotropy of electrical resistivity, $\rho_a(T)/\rho_{bc}(T)$, increases with decreasing temperature from 17 at 305 K to 50 at 1.8 K, which implies the electronic structure is quasi-two-dimensional in $CaMnSb_2$. Figure 4(b) shows the temperature dependence of in-plane resistivity $\rho_{bc}(T)$ in the fields of 0 and 9 T for $B\|a$ and $B\|bc$, respectively. The application of magnetic fields enhances the value of $\rho_{bc}(T)$. The magnetoresistance MR $= [\rho_{bc}(B) - \rho_{bc}(0)]/\rho_{bc}(0)]$ is less than 2% at $T = 305$ K and $B = 9$ T for both $B\|a$ and $B\|bc$. While with the temperature decreasing, the MR increases gradually and shows a strong anisotropy, which can reach as high as about 396% for $B\|a$ at 1.8 K in a magnetic field of 9 T, but there is only a small increase to 19% for $B\|bc$. The magnetic field dependence of MR, displayed in Fig. 4(c), shows quasilinear behavior. Large positive quasilinear MR is also observed in Dirac materials such as $AMnBi_2$ [13–20] and $AMnSb_2$ [34,35], which is ascribed to the linear energy dispersion in the electronic band structure. At high magnetic field, MR for $B\|a$ deviates slightly

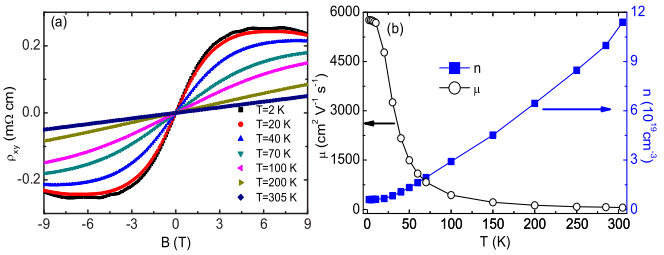

FIG. 5. (a) The magnetic field dependence of Hall resistivity ρ_{xy} at various temperatures from 2 to 305 K. (b) Temperature dependence of carrier density and mobility.

from the quasilinear behavior and shows weak Shubnikov-de Haas (SdH) oscillations. We can obtain two fundamental frequencies of 7.8 and 14.4 T from the FFT analysis of SdH oscillations, which are consistent with the results of dHvA effect. We also measured the angular-dependent ρ_{bc} at 1.8 K in a magnetic field of 9 T [Fig. 4(d)], which shows a maximum value at $B\|a$ ($\theta = 0$, 180, and 360°) and a minimum value at $B\|bc$ ($\theta = 90$ and 270°). We found that the whole curve of angular-dependent ρ_{bc} accords with the function of $|\cos\theta|$ very well, confirming the electronic structure is quasi-two-dimensional in $CaMnSb_2$.

Figure 5(a) depicts the magnetic field dependence of Hall resistivity ρ_{xy} at various temperatures. At high temperatures, ρ_{xy} exhibits linear field dependence, while at low temperatures ρ_{xy} shows obvious downward curvature, suggesting $CaMnSb_2$ is a multicarrier system. At low temperatures and high magnetic fields, ρ_{xy} is accompanied by weak SdH oscillations. It is clearly shown that Hall coefficient $R_H = \rho_{xy}(T)/B$ is positive at all temperatures, which implies the dominant charge carriers are holes in $CaMnSb_2$. For the sake of simplicity, we used a single-band model to estimate carrier density $n = 1/eR_H$ and carrier mobility $\mu = R_H/\rho_{xx}(0\ \mathrm{T})$, where R_H was estimated by the slope of $\rho_{xy}(B)$ at low fields ($-1 < B < 1$ T). Figure 5(b) shows the temperature dependence of carrier density and mobility. The carrier density decreases from 1.1×10^{20} cm^{-3} at 305 K to 6×10^{18} cm^{-3} at 2 K, but the carrier mobility increases from 57 cm^2 V^{-1} s^{-1} at 305 K to 5764 cm^2 V^{-1} s^{-1} at 2 K. The carrier density and mobility are similar to $AMnBi_2$ and (Sr/Ba)$MnSb_2$ [13–19,34,35], which are in accord with the existence of Dirac fermions in $CaMnSb_2$.

In summary, we have reported the electrical transport properties and quantum oscillations in high-quality single crystals of $CaMnSb_2$. The results show that $CaMnSb_2$ is an antiferromagnetic metal with a quasi-two-dimensional electronic structure. The Hall effect indicates that $CaMnSb_2$ is a multiband system and the electronic transport is dominated by holelike charge carriers. The nontrivial Berry phase, small cyclotron mass, and high carrier mobility imply that nearly massless Dirac fermions host in $CaMnSb_2$. The smaller cross-sectional area of the FS and tiny cyclotron effective mass suggest Dirac band crossing points may be closer to the Fermi level in $CaMnSb_2$.

This work was supported by the Natural Science Foundation of China (Grant No. 11404175), the National

Basic Research Program of China 973 Program (Grant No. 2015CB921303), the National Key Research Program of China (Grant No. 2016YFA0300604), the Strategic Priority Research Program (B) of Chinese Academy of Sciences (Grant No. XDB07020100), the Innovation Scientists and Technicians Troop Construction Projects of Henan Province (Grant No. C20150029), Youth Funded Projects of Nanyang Normal University (Grant No. QN2016009), the Key Scientific and Technological Project of Technology Department of Henan Province (Grant No. 162102210305), and the Science Fund of Educational Department of Henan Province (Grant No. 15A140030).

[1] A. H. Castro Neto, F. Guinea, N. M. R. Peres, K. S. Novoselov, and A. K. Geim, Rev. Mod. Phys. **81**, 109 (2009).
[2] M. Z. Hasan and C. L. Kane, Rev. Mod. Phys. **82**, 3045 (2010).
[3] A. Bansil, H. Lin, and T. Das, Rev. Mod. Phys. **88**, 021004 (2016).
[4] Y. B. Zhang, Y. W. Tan, H. L. Stormer, and P. Kim, Nature (London) **438**, 201 (2005).
[5] K. S. Novoselov, Z. Jiang, Y. Zhang, S. Morozov, H. Stormer, U. Zeitler, J. C. Maan, G. S. Boebinger, P. Kim, and A. K. Geim, Science **315**, 1379 (2007).
[6] T. Liang, Q. Gibson, M. N. Ali, M. Liu, R. J. Cava, and N. P. Ong, Nat. Mater. **14**, 280 (2015).
[7] J. Xiong, S. K. Kushwaha, T. Liang, J. W. Krizan, M. Hirschberger, W. D. Wang, R. J. Cava, and N. P. Ong, Science **350**, 413 (2015).
[8] H. Weng, C. Fang, Z. Fang, B. A. Bernevig, and X. Dai, Phys. Rev. X **5**, 011029 (2015).
[9] S.-Y. Xu, I. Belopolski, N. Alidoust, M. Neupane, G. Bian, C. Zhang, R. Sankar, G. Chang, Z. Yuan, C.-C. Lee, S.-M. Huang, H. Zheng, J. Ma, D. S. Sanchez, B. Wang, A. Bansil, F. Chou, P. P. Shibayev, H. Lin, S. Jia, and M. Z. Hasan, Science **349**, 613 (2015).
[10] B. Q. Lv, H. M. Weng, B. B. Fu, X. P. Wang, H. Miao, J. Ma, P. Richard, X. C. Huang, L. X. Zhao, G. F. Chen, Z. Fang, X. Dai, T. Qian, and H. Ding, Phys. Rev. X **5**, 031013 (2015).
[11] X. Huang, L. Zhao, Y. Long, P. Wang, D. Chen, Z. Yang, H. Liang, M. Xue, H. Weng, Z. Fang, X. Dai, and G. Chen, Phys. Rev. X **5**, 031023 (2015).
[12] C. L. Zhang, S. Y. Xu, I. Belopolski, Z. J. Yuan, Z. Q. Lin, B. B. Tong, G. Bian, N. Alidoust, C. C. Lee, S. M. Huang, T. R. Chang, G. Q. Chang, C. H. Hsu, H.-T. Jeng, M. Neupane, D. S. Sanchez, H. Zheng, J. F. Wang, H. Lin, C. Zhang, H. Z. Lu, S. Q. Shen, T. Neupert, M. Z. Hasan, and S. Jia, Nat. Commun. **7**, 10735 (2016).
[13] J. Park, G. Lee, F. Wolff-Fabris, Y. Y. Koh, M. J. Eom, Y. K. Kim, M. A. Farhan, Y. J. Jo, C. Kim, J. H. Shim, and J. S. Kim, Phys. Rev. Lett. **107**, 126402 (2011).
[14] K. F. Wang, D. Graf, L. M. Wang, H. C. Lei, S. W. Tozer, and C. Petrovic, Phys. Rev. B **85**, 041101 (2012).
[15] L. J. Li, K. F. Wang, D. Graf, L. M. Wang, A. F. Wang, and C. Petrovic, Phys. Rev. B **93**, 115141 (2016).
[16] Y. Y. Wang, Q. H. Yu, and T. L. Xia, Chin. Phys. B **25**, 107503 (2016).
[17] A. Wang, I. Zaliznyak, W. Ren, L. Wu, D. Graf, V. O. Garlea, J. B. Warren, E. Bozin, Y. Zhu, and C. Petrovic, Phys. Rev. B **94**, 165161 (2016).
[18] K. F. Wang, D. Graf, H. C. Lei, S. W. Tozer, and C. Petrovic, Phys. Rev. B **84**, 220401 (2011).
[19] A. F. May, M. A. McGuire, and B. C. Sales, Phys. Rev. B **90**, 075109 (2014).
[20] J. B. He, D. M. Wang, and G. F. Chen, Appl. Phys. Lett. **100**, 112405 (2012).
[21] S. Borisenko, D. Evtushinsky, Q. Gibson, A. Yaresko, T. Kim, M. N. Ali, B. Buechner, M. Hoesch, and R. J. Cava, arXiv:1507.04847 (2015).
[22] L. L. Jia, Z. H. Liu, Y. P. Cai, T. Qian, X. P. Wang, H. Miao, P. Richard, Y. G. Zhao, Y. Li, D. M. Wang, J. B. He, M. Shi, G. F. Chen, H. Ding, and S. C. Wang, Phys. Rev. B **90**, 035133 (2014).
[23] G. Lee, M. A. Farhan, J. S. Kim, and J. H. Shim, Phys. Rev. B **87**, 245104 (2013).
[24] Y. Feng, Z. J. Wang, C. Y. Chen, Y. G. Shi, Z. J. Xie, H. M. Yi, A. J. Liang, S. L. He, J. F. He, Y. Y. Peng, X. Liu, Y. Liu, L. Zhao, G. D. Liu, X. L. Dong, J. Zhang, C. T. Chen, Z. Y. Xu, X. Dai, Z. Fang, and X. J. Zhou, Sci. Rep. **4**, 5385 (2014).
[25] H. Masuda, H. Sakai, M. Tokunaga, Y. Yamasaki, A. Miyake, J. Shiogai, S. Nakamura, S. Awaji, A. Tsukazaki, H. Nakao, Y. Murakami, T. hisa Arima, Y. Tokura, and S. Ishiwata, Sci. Adv. **2**, e1501117 (2016).
[26] J. K. Wang, L. L. Zhao, Q. Yin, G. Kotliar, M. S. Kim, M. C. Aronson, and E. Morosan, Phys. Rev. B **84**, 064428 (2011).
[27] Y. F. Guo, A. J. Princep, X. Zhang, P. Manuel, D. Khalyavin, I. I. Mazin, Y. G. Shi, and A. T. Boothroyd, Phys. Rev. B **90**, 075120 (2014).
[28] Y. J. Jo, J. Park, G. Lee, M. J. Eom, E. S. Choi, J. H. Shim, W. Kang, and J. S. Kim, Phys. Rev. Lett. **113**, 156602 (2014).
[29] Y. Ishida, H. Masuda, H. Sakai, S. Ishiwata, and S. Shin, Phys. Rev. B **93**, 100302 (2016).
[30] K. F. Wang, L. M. Wang, and C. Petrovic, Appl. Phys. Lett. **100**, 112111 (2012).
[31] M. Chinotti, A. Pal, W. J. Ren, C. Petrovic, and L. Degiorgi, Phys. Rev. B **94**, 245101 (2016).
[32] J. Y. Liu, J. Hu, D. Graf, T. Zou, M. Zhu, Y. Shi, S. Che, S. M. A. Radmanesh, C. N. Lau, L. Spinu, H. B. Cao, X. Ke, and Z. Q. Mao, arXiv:1608.05956 (2016).
[33] M. A. Farhan, G. Lee, and J. H. Shim, J. Phys.: Condens. Matter **26**, 042201 (2014).
[34] J. Y. Liu, J. Hu, H. B. Cao, Y. L. Zhu, A. Chuang, D. Graf, D. J. Adams, S. M. A. Radmanesh, L. Spinu, I. Chiorescu, and Z. Q. Mao, Sci. Rep. **6**, 30525 (2016).
[35] J. Y. Liu, J. Hu, Q. Zhang, D. Graf, H. B. Cao, S. M. A. Radmanesh, D. J. Adams, Y. L. Zhu, G. F. Cheng, X. Liu, W. A. Phelan, J. Wei, D. A. Tennant, J. F. DiTusa, I. Chiorescu, L. Spinu, and Z. Q. Mao, arXiv:1507.07978 (2015).
[36] E. Brechtel, G. Cordier, and H. Schäfer, J. Less Common Metals **79**, 131 (1981).
[37] I. M. Lifshitz and A. M. Kosevich, Zh. Eksp. Teor. Fiz. **29**, 730 (1955) [Sov. Phys. JETP **2**, 636 (1956)].
[38] A. R. Wright and R. H. McKenzie, Phys. Rev. B **87**, 085411 (2013).